

A CGPS LOOK AT THE SPIRAL STRUCTURE OF THE OUTER MILKY WAY I: DISTANCES AND VELOCITIES TO STAR FORMING REGIONS

TYLER J. FOSTER^{1,2}Department of Physics & Astronomy, Brandon University, Brandon, Manitoba, Canada and
National Research Council Canada, Penticton, British Columbia, Canada

AND

CHRISTOPHER M. BRUNT³Astrophysics Group, School of Physics, University of Exeter, Exeter, United Kingdom
(Received 2014 May 16)

ABSTRACT

We present a new catalogue of spectrophotometric distances and line-of-sight systemic velocities to 103 H II regions between $90^\circ \leq \ell \leq 195^\circ$ (longitude quadrants II and part of III). Two new velocities for each region are independently measured using 1-arcminute resolution 21 cm H I and 2.6 mm ¹²CO line maps (from the Canadian Galactic Plane Survey and FCRAO Outer Galaxy Surveys) that show where gaseous shells are observed around the periphery of the ionized gas. Known and neighbouring O&B-type stars with published UBV photometry and MK classifications are overlaid onto 21 cm continuum maps, and those stars observed within the boundary of the H II emission (and whose distance is not more than 3 times the standard deviation of the others) are used to calculate new mean stellar distances to each of the 103 nebulae. Using this approach of excluding distance outliers from the mean distance to a group of many stars in each H II region lessens the impact of anomalous reddening for certain individuals. The standard deviation of individual stellar distances in a cluster is typically 20% per stellar distance, and the error in the mean distance to the cluster is typically $\pm 10\%$. Final mean distances of 9 common objects with VLBI parallax distances show a 1:1 correspondence. Further, comparison with previous catalogues of H II regions in these quadrants shows a 50% reduction in scatter for the distance to Perseus spiral arm objects in the same region, and a reduction by $\sim 1/\sqrt{2}$ in scatter around a common angular velocity relative to the Sun $\Omega - \Omega_0$ (km s⁻¹ kpc⁻¹). The purpose of the catalogue is to provide a foundation for more detailed large-scale Galactic spiral structure and dynamics (rotation curve, density wave streaming) studies in the 2nd and 3rd quadrants, which from the Sun's location is the most favourably viewed section of the Galaxy.

Keywords: HII regions — ISM: kinematics and dynamics — Galaxy: structure — Galaxy: kinematics and dynamics

1. INTRODUCTION

The utility of H II regions as tracers of Galactic spiral structure and rotation is well-known. Some of today's most successful models of our Galaxy (e.g. the electron-density model of Taylor & Cordes 1993, and the dust model of Drimmel & Spergel (2001)) are based on the H II arms originally mapped by Georgelin & Georgelin (1976). Distances to H II regions and their attendant molecular clouds can be obtained photometrically with broadband and spectroscopic data on internal exciting stars, and/or kinematically via the object's systemic velocity. The classic map of Georgelin & Georgelin (1976) uses both methods, as does very recent work to produce global maps of spiral structure (e.g. Hou et al. 2009; Russeil 2003) or more detailed spiral structure maps in smaller areas across the Galactic plane (e.g.

Vázquez et al. 2008). Neither method can approach the accuracy typical of VLBI/parallax observations (e.g. Xu et al. 2006) but large-scale mapping efforts with this method are only just beginning (see Brunthaler et al. 2011, for a good review, though this method too can be quite uncertain; see Miyoshi et al. (2012)).

In particular, spiral structure in the 2nd and 3rd quadrants of longitude (QII and QIII; $90^\circ \leq \ell \leq 270^\circ$), our nearest view of the Outer Galaxy, is uncertain. Arms are moderately well-defined to about $R \sim 10$ kpc (e.g. see Reid et al. 2009), with most maps distinguishing the Local arm (a steeply-pitched spur or “armlet” that the Sun seems to be a member of) from the Perseus arm (a major tightly-wound star-forming arm, the closest such arm to the Sun). Beyond 2-3 kpc from the Sun in QII and QIII, most maps presented thus far become quite ill-defined. The modern consensus of spiral structure rendered in Churchwell et al. (2009) (principally based on Georgelin & Georgelin) shows one arm beyond Perseus, the “Outer” arm, some ~ 6.1 kpc distant from the Sun towards $\ell = 180^\circ$, and placed there to kinematically link with the QIII arm of McClure-Griffiths et al. (2004) in the Outer Galaxy and linking to the Norma arm in the Inner Galaxy QIV. In ¹²CO $\ell - v$ maps by Dame et al. (2001) this Outer arm is a sparse chain of clouds that

FosterT@BrandonU.CA
brunt@astro.ex.ac.uk

¹ Department of Physics & Astronomy, Brandon University, 270-18th Street, Brandon, MB, R7A 6A9 Canada

² National Research Council of Canada, Emerging Technologies – National Science Infrastructure, Dominion Radio Astrophysical Observatory, P.O. Box 248, Penticton BC, V2A 6J9, Canada

³ Astrophysics Group, School of Physics, University of Exeter, Stocker Road, Exeter, EX4 4QL, United Kingdom

appears somewhat coherent over a wide range of longitude. Strasser et al. (2007) also trace this arm kinematically using continuum absorption towards extragalactic sources. Discrete tracers beyond Perseus in this area are also shown in Vázquez et al. (2008) but their fit with the Outer arm (as defined by the “Cygnus” arm of Vallée 2008) is very poor. While these distant tracers suffer from high scatter, if anything their mean position seems to be somewhat closer to the Sun than the Cygnus Arm of Vallée (2008), and are more consistent as belonging to the optical arm suggested by Kimeswenger & Weinberger (1989) and Negueruela & Marco (2003), which at 4–5 kpc from the Sun towards $\ell = 180^\circ$ is nearer than the Cygnus arm of Vallée (2008) and the Outer arm of Churchwell et al. (2009). This arm is positioned 3.5 kpc towards $\ell = 180^\circ$ in the 4-arm model of Hou et al. (2009) though it is poorly defined and not linked to any arms in the Inner Galaxy. Beyond the Cygnus arm, there is unreliable evidence for an even more distant Far Outer arm some 7–9 kpc from the Sun towards 180° (e.g. Vallée 2008; Hou et al. 2009). Such an arm could be a QII-extension of the Scutum-Centaurus arm identified in the 1st quadrant by Dame & Thaddeus (2011). While it is proposed by Churchwell et al. (2009) and Dame & Thaddeus (2011) that this arm along with Perseus forms the principal 2-armed density wave pattern emanating from the central bar in the MW, the picture is still not clear (see the synopsis of spiral structure in Vallée 2008, which shows the Perseus arm as a secondary arm).

Clearly then, the view of the overall Milky Way spiral structure and how the pattern in QII and QIII relates to it is (as yet) incomplete and conflicted. In particular a more precise location and winding angle for the QII/QIII arms would help to mate the patterns and visualize the big picture. The challenge then is to refine distances to spiral arm tracers and to minimize their uncertainties, with a more rigorous and systematic approach to spectro-photometric distances to stars, and/or better defined measurements of the *systemic* velocities of tracers. That is the broad purpose of this series of papers.

There are three major obstacles to a better defined map of spiral structure from H II region distances. First and most major are distance uncertainties, sources for which are i) misclassification of spectral and MK types for exciting stars, ii) errors in photometry, iii) variation in intrinsic luminosity for stars of the same class, and iv) a changing reddening law for stars that are seen through different relative amounts of interstellar and circumstellar dust. Second, data are cobbled together from inhomogeneous sets of published catalogues and groups of nebula with different distance estimates used for each (as noted, often a mix of kinematic and spectrophotometric), the differences among them being constants used (e.g. Solar galactocentric distance R_0), the calibrations of MK/spectral type vs. intrinsic colour and magnitudes, and even the identity and the number of stars considered involved with a given H II region. Thirdly, it is not necessary that all observed H II regions must also be tracing a major spiral feature; hence any spiral structure present may appear confused by the presence of interarm objects and other objects not associated with the major arms.

Maps made with kinematic distances of H II regions are also affected by a major source of error: deviations

of the observed velocity of a tracer from circular Galactic rotation. These can come in the form of larger-scale systematic non-circular motions like elliptical orbits, and spiral arm dynamics (e.g. streaming motions associated with density waves, and “rolling” motions that are observed in spiral arms Roberts 1972; Feitzinger & Spicker 1985, respectively), down to smaller-scale motions like expansions of gaseous shells surrounding the stars, molecular and champagne-type outflows associated with many SFRs, and down to the very-small scale random turbulent motions associated with the gas. Even such small non-circular deviations can be magnified by the $1/\sin\ell$ projection of circular velocities in QII and QIII.

The new catalogue presented here (Paper I) is the foundation for a series of following papers that have two purposes; Paper II) clarifies and refines the spatial spiral structure in the Outer Galaxy’s 2nd and 3rd quadrants, and Paper III) refines the observed rotation curve and resolves new detailed spiral arm dynamics within it. These goals are accomplished by specifically addressing many of the sources of uncertainty noted above. Specifically, these papers improve upon the following sources: 1) errors in distances due to random measurement errors (such as errors in photometry) and random variations in absolute magnitudes and colours among common stellar types, 2) scatter due to inhomogeneity in parameters/calibrations used to calculate distances, 3) errors in velocities due to expanding shells and outflows along the line-of-sight, and 4) errors in velocities due to random turbulent motions. Specifically, the next paper (II) will further address 5) scatter in spiral structure maps caused by uncertainty in the association of each H II region with spiral arms or interarm regions, and Paper III will address 6), the scatter in the rotation curve caused by systematic large-scale “rolling” (i.e. z -dependent) motions.

The new catalogue contains 103 H II regions observed by the Canadian Galactic Plane Survey (CGPS, Taylor et al. 2003) in the region $90^\circ \leq \ell \leq 195^\circ$, each with a compilation of associated and nearby (on the sky) OB stars with spectral classes and UBV photometric measurements, as complete as the current literature to 2013 allows. To minimize source 1) above, new group distances for each H II region are calculated using typically more stars than are usually used for each nebula, but only those that meet several objective spatial criteria for association. To minimize source 2) the same modern magnitude-luminosity and colour index $(B - V)_0$ calibrations are used for the whole sample. To address source 3) systemic velocities with respect to the LSR are found for each H II region by using high-resolution CGPS line data and looking for velocity channels where associated shells and clouds are resolved edge-on with respect to the ionized gas, and not face-on. Finally random velocity variations (source 4 above) from turbulent and cloud-cloud dispersion motions are minimized by deriving two independent velocity estimates, from both H I and CO maps for each H II region. These efforts result in a more homogeneous, meaningful, and most importantly repeatable set of H II region distances and velocities. In Papers II and III that follow this catalogue, we deal with sources of uncertainty due to 5) and 6) respectively.

2. OBSERVATIONS AND METHOD

The cornerstone of our catalog of H II regions is the new systemic velocity measurements (with respect to the LSR), which come from high-resolution (1 arcminute) $\lambda 21$ cm H I data and $\lambda 2.6$ mm $^{12}\text{CO}(J=1 \rightarrow 0)$ data. The H I data are entirely from the Canadian Galactic Plane Survey (CGPS; Taylor et al. 2003), whereas CO data are from either CGPS or the Exeter FCRAO CO Galactic Plane Survey (described in Mottram & Brunt 2010; Brunt et al. 2013), depending on longitude. Our catalog covers H II regions in the Outer Galaxy only ($R > R_0$) in the longitude range $90^\circ \leq \ell \leq 193^\circ$ and mainly within a latitude of $-3.5^\circ \leq b \leq +5.5^\circ$. A high-latitude extension was also observed as part of the CGPS ($99^\circ 85' \leq \ell \leq 116^\circ 96'$) up to $b = +17^\circ 56'$. The complete CGPS dataset of 21 cm line and continuum from $50^\circ 2' \leq \ell \leq 193^\circ 3'$ and $-3^\circ 55' \leq b \leq +5^\circ 55'$ are available at the Canadian Astronomy Data Centre⁴.

2.1. H I Line Observations

21 cm H I line observations used herein were carried out with the 7-element interferometer and 26 metre radio telescopes at the Dominion Radio Astrophysical Observatory (DRAO) for the CGPS. The final line data product are 5.1×5.1 H I datacubes, which have $\simeq 1$ arcminute resolution in each of 256 channel maps separated by 0.824 km s^{-1} and of 1.32 km s^{-1} resolution. The line data have a brightness-temperature sensitivity of $\Delta T_B = 3.5 \sin \delta$ K. More information on the CGPS observing and data processing strategy may be found in Taylor et al. (2003).

2.2. CO Line Observations

To trace molecular material in the Second Quadrant, we make use of the Five College Radio Astronomy Observatory (FCRAO) Outer Galaxy Survey (OGS; Heyer et al. 1998). The OGS mapped $^{12}\text{CO } J=1-0$ spectral line emission over the longitude range $102^\circ 5' \leq \ell \leq 141^\circ 5'$ and over latitudes $-3^\circ 0' \leq b \leq +5^\circ 4'$. For regions outside the OGS coverage, we use new FCRAO CO surveys: the Extended Outer Galaxy Survey (E-OGS) extends the coverage of the OGS to Galactic longitude $\ell = 193^\circ$, over a latitude range $-3^\circ 5' \leq b \leq +5^\circ 5'$; and a new survey in the Cygnus region connects the OGS to the Galactic Ring Survey (GRS; Jackson et al. 2006) between longitudes $55^\circ 7' \leq \ell \leq 102^\circ 5'$, over the (approximate) latitude range $-1^\circ 0' \leq b \leq +1^\circ 25'$. Full details of these new surveys are reported elsewhere (Brunt et al. in prep.) and are briefly summarized here. All new surveys utilised the 32 pixel SEQUOIA focal plane array (Erickson et al. 1999) to image the ^{12}CO and $^{13}\text{CO } J=1-0$ spectral lines at ~ 45 arcsecond angular resolution in the on-the-fly (OTF) mapping mode. The two lines were acquired simultaneously by the dual channel correlator (DCC), configured with 1024 channels over a bandwidth of 50 MHz at each frequency. The total velocity coverage exceeds 120 km s^{-1} , and is centered on $v_{\text{LSR}} = -40 \text{ km s}^{-1}$ over the range of longitudes examined in this paper. The channel spacing is 0.126 km s^{-1} (^{12}CO) and 0.132 km s^{-1} (^{13}CO); the velocity resolution is broader by a factor of 1.21. ^{12}CO OGS data prepared for inclusion in the CGPS were smoothed to

1.319 km s^{-1} , and new E-OGS data are smoothed to this resolution as well before analysis in this study. During the survey observations, pointing and focus checks were carried out every 3-4 hours, shortly after dawn/dusk or after a significant change in source coordinates. The data were initially converted to the T_A^* scale using the standard chopper wheel method (Kutner & Ulich 1981). We used the OTFTOOL software, written by M. Heyer, G. Narayanan, and M. Brewer, to place the spectra on a regular $22.5''$ grid in Galactic ℓ , b coordinates. To achieve this, first order baselines were fitted to signal-free regions of each spectrum and the root mean square noise amplitude (σ) of each spectrum was recorded. After baseline removal, individual spectra contributing to a single Galactic coordinate were assigned a $1/\sigma^2$ weighting during the gridding. The gridded data were scaled to the radiation temperature scale (T_R^*) by dividing by $\eta_{\text{FSS}} = 0.7$ to account for forward scattering and spillover losses.

3. IDENTIFYING EXCITING STARS

An extensive search of the CGPS 21 cm continuum data was conducted to identify known bright H II regions. We find 103 objects, including most of the objects in Sharpless' second catalogue (Sharpless 1959) that fall within the CGPS survey area, and most of which have known associated stars from a set of standard catalogs: Georgelin & Georgelin (1970); Georgelin et al. (1973); Crampton et al. (1978); Moffat et al. (1979); Chini & Wink (1984); Avedisova & Kondratenko (1984); Hunter & Massey (1990); Glushkov (1995); Russeil et al. (2007). In some studies exciting stars have been identified from deep observations of a particular nebula (Sh2-138 and Sh2-184, in Deharveng et al. 1999; Guetter & Turner 1997, respectively), or smaller samples of nebulae (Lahulla 1985, 1987). However, to expand the list of known stars associated with each H II region (especially the larger diffuse ones), we follow a systematic procedure.

We begin with $1'$ -resolution 21 cm continuum emission maps of each H II region from the CGPS, contoured (typically 1,3,5 Kelvin levels above the background) to clearly delineate the boundaries of the ionized gas. Where 21 cm emission is not well defined or not detected at all we also use $\text{H}\alpha$ emission contoured from the composite map of Finkbeiner (2003). Known exciting stars from the standard catalogs above are first overlaid, showing positions with respect to the continuum emission. Then, we searched around the centre of this emission in SIMBAD for additional OB-type stars not reported in the "standard" catalogues. Our main source for additional OB stars in the area is the catalogue of Reed (2003) (and references therein), with some additional stellar classes and photometry from smaller catalogues of observations of specific stars and Galactic plane regions (Martin 1972; Crampton & Fisher 1974; Hill & Lynas-Gray 1977; Wramdemark 1981; Massey et al. 1995; Negueruela & Marco 2003; Sota et al. 2011). Candidates for association were those stars whose position was within or reasonably near to the outermost 21 cm continuum or $\text{H}\alpha$ emission boundary. Mainly those with UBV photometry and published spectral types of O3 to B4 were considered. Where they exist we also consider Tycho B-type stars

⁴ CADC; <http://cadc.hia.nrc.ca>

which have no assigned numerical sub-type.

Next, spectroscopic distances to all known and candidate stars are calculated from their photometry, spectral types and luminosity classes. Distances for all stars use reddenings $E(B - V) = (B - V) - (B - V)_0$ that are calculated from the modern spectral type-intrinsic colour calibration referred to in Pecaut et al. (2012) (for main sequence stars) and Wegner (1994) (for luminosity classes I-IV). Absolute magnitudes are from the M_V calibration compiled by Russeil (2003). Both of these calibrations are reproduced at the end of in Table 1. A value $R_V = 3.2$ for the ratio of total-to-differential interstellar extinction is assumed throughout (Fitzpatrick & Massa 2007). Where multiple values for magnitude V , colours $B - V$, $U - B$, spectral types, and MK Luminosity Classes (LC Ia-V) are listed in Reed (2003) we invariably use the more recent published ones. If no LC is given, we use the next most recent published one, and if none at all are known we assume the star is LCV (main sequence). If the star has only been classed as a B-type star from Tycho photometry, we assume LCV, calculate its reddening free index $Q = (U - B) - 0.72(B - V)$ and estimate its sub-type (B0-B4) from Henden & Kaitchuck (1990). As a last resort in three cases (Sh2-134, 147, 166) where a single OB type star with only B and V photometry is present but no temperature or luminosity class is known, we assume LCV and estimate the spectral type from the ratio of 21 cm radio flux and total IR flux (e.g. Chan & Fich 1995, or measured with reprocessed IRAS data in the CGPS), a distance-independent method originally proposed by Dewdney et al. (1991) that involves estimating the number of ionizing photons N_{rad} (photons s^{-1}) from the nebula's radio flux S_ν (Jy) (e.g. see equation p.853 Hunter & Massey 1990, with T_e assumed $\simeq 10^4$ K) and the IR luminosity $L_{IR}(L_\odot)$ and comparing their ratio (which is distance-independent but well calibrated with model stellar type; e.g. in Sternberg et al. 2003). The method assumes the ionizing flux from the embedded star(s) is entirely reprocessed into IR luminosity, and results in an upper-limit to the spectral type of the star(s) within.

For a robust mean distance estimate to each nebula we attempt to minimize the impact of uncertain stellar distances and unrelated stars. With a set of 355 stars potentially associated with the 103 nebulae, we use an objective procedure of excluding candidates from the mean distance estimate. We consider all three dimensions: i) two on the plane of the sky in ℓ , b , and ii) the third in depth/distance r . The first two dimensions are filtered by excluding stars on the plane of the sky that are not seen within the boundaries of the ionized gas (21 cm and/or H α emission contours), and as well are not found inside H I and/or CO gas shells/walls that surround each nebula. The third dimension (depth) is screened by excluding stars have conspicuous and excessively different distances that are $\sim 3\sigma$ or more away from the mean distance to the other members and candidates. Combinations of both i) and ii) are also screened. Examples of excluded stars are shown in Figures 3 and 2 (see Sec. 4), marked with x-symbols; one star in Sh2-204, and one each in the centres of Sh2-207 and 208 with $\geq 3\sigma$ distance differences from the others, one star north of Waterloo 1 and four stars around Sh2-173 excluded by

their position outside of the continuum emission and associated H I and ^{12}CO shells, and one star in Sh2-168 by both its outlying position and distance. Stars that were borderline to meeting i) were additionally scrutinized by their published radial velocity (if available); those with a similar velocity to the nebula ($\lesssim 20 \text{ km s}^{-1}$ different) were included. Finally, for three nebulae (Sh2-193, 203 and 232) only two stars are associated with very different distances; we choose the single star whose distance is closest to the group of H II regions that these objects belong to (i.e. Sh2-192 to 196, Sh2-203 to BFS 31, and Sh2-231 to 235 respectively). Applying the above criteria, we cull some 45 stars from our list.

We present our full catalogue of 355 stars found in and around Galactic H II regions online in both Excel sheet and PDF formats; see <ftp://ftp.drao.nrc.ca/pub/users/foster/Table1.xls> or [/Table1.pdf](#). A sample of Table 1 is reproduced below. The 45 stars excluded by the criteria above are marked in Table 1 for clarity, but do not contribute to the final distance calculation. The final tally of stars we associate spatially with 21 cm continuum from each of 103 H II regions is 310. 205 have been classified as LCV in the literature from spectra, and 44 have been assumed (mainly in the literature, or by us) LCV for the distance calculation. Among them, 23 B-type stars have spectral subtypes estimated from the Q index; one or more stars in the following H II regions: Sh2-129, CTB 104b, 154, BFS 17, 157, 163, 170(2), 173(2), 177(3), 199, 204(2), 207(2), 208/Waterloo 1(2), 249(2), and 259. The number distribution of spectral types among O3-B4V stars is plotted in Figure 1, and shows that the most common main sequence star in our sample is type B1.

Table 2 in this paper gives the final heliocentric stellar distance $r \pm dr$ to each of 103 nebulae in the Outer Galaxy. We also include mean stellar distances calculated to seven additional H II regions (associated with 10 additional stars) just outside the CGPS high-longitude border (Sh2-261, and Sh2-267 through 272). Although these objects could not be scrutinized in the same way as regions observed in the CGPS 21 cm maps and (thus) are not part of our main catalogue, Sh2-267 - 272 in particular are an important cluster of six H II regions tracing the extension of the Cygnus spiral arm into the 3rd quadrant (discussed in Paper II), so their distances are presented here for use later on.

3.1. Distance Uncertainties

56 of the nebulae (including two groups at a common distance: Sh2-156+BFS 17, and Sh2-254-258, and three non-CGPS H II regions beyond $\ell = 193^\circ$) have two or more associated stars identified (Column 8 in Table 2; numbers in brackets are the number of excluded stars), so uncertainties in the mean distance to the H II region can be assessed directly with the standard deviation of stellar distances in a cluster of n_* stars as $\sigma_*/\sqrt{n_*}$. Here σ_* is the standard deviation of the stars' distances, or the average uncertainty in an individual star's distance. The distributions of distance uncertainties (as a percent of the mean distance to the cluster), both per star and for the mean distance to the group are shown in Figure 1. The errors in the mean distances fairly follow a normal distribution with a small positive skew, peaking

Table 1

Sample lines from full Table 1 online at <ftp://ftp.drao.nrc.ca/pub/users/foster/Table1.pdf>. The online version also contains star names, coordinates, references, and descriptions.

Object	ℓ (deg.)	b (deg.)	v_{CO} (km s ⁻¹)	v_{HI} (km s ⁻¹)	$v_{H\alpha}$ (km s ⁻¹)	$\langle r \rangle$ (kpc)	ΔD / $\langle r \rangle$	E(B-V) (mag.)	V (mag.)	(B-V) mag.	Spec Type	LC	(B-V) ₀ mag.	M(R03) mag.
Sh2-121	90.23	1.72	-62.4	-56.7	-61.1	6.82	0.05	2.08 2.066 1.92	14.91 15.44 15.48	1.86 1.76 1.76	B0 O4 B2	II V II	-0.22 -0.306 -0.16	-5.75 -5.52 -4.8
Sh2-124	94.57	-1.45	-43.6	-41.865	-37	3.78	0.17	1.248 1.39	12.28 14.46	0.95 1.18	O7 B2	V V	-0.298 -0.21	-4.94 -2.47
CTB104b	94.72	-1.54	-15.0 -41.0	-14.65		2.36	0.06	0.62 0.3 0.82 0.81 0.41	11.36 9.97 10.73 9.62 9.06	0.37 0.09 0.52 0.51 0.11	B1.5 B2 B0 O7.5 B0	V V V V V	-0.25 -0.21 -0.3 -0.3 -0.3	-2.81 -2.47 -3.9 -4.88 -3.9
Sh2-127	96.27	2.57	-94.7	-92.98	-98.9	9.97		1.73	15.80	1.44	O8	V	-0.29	-4.73
BFS8	96.35	-0.2	-57.5	-55.47		8.75		1.338	13.58	1.035	O5	V	-0.303	-5.41
Sh2-128	97.56	3.16	-74.0	-70.72	-76.8	8.06		1.768	15.25	1.47	O7	V	-0.298	-4.94
Sh2-129	99.06	7.4	1.4	-6.3 Cep OB2	-8	0.81	0.18	0.38 0.368 0.4 1.06 0.65	6.09 8.14 9.21 11.17 8.63	0.08 0.19 0.19 0.85 0.44	B0 B3 B2 B2 B2	V V V V V	-0.3 -0.178 -0.21 -0.21 -0.21	-3.9 -1.6 -2.47 -2.47 -2.47

at $\sim \pm 10\%$ of the mean distance, and range from $\leq 2\%$ to 30%. Note that the errors defining these distributions include contributions from random errors in photometry and errors in spectral classification (temperature and luminosity classes), but not from systematic differences caused by, for example, an anomalous extinction law (i.e. $R_V = A_V/E(B-V) > 3.2$ for dust of different grain size than that typical of the ISM), which is not a normally-distributed error. This will cause additional scatter towards higher distances and potentially create some dramatically outlying distances (dealt with by robust statistics in Paper II). All other nebulae have only one identified stellar member and their distances are assigned $\sim \pm 20\%$, the average standard deviation per star in all groups of two or more stars.

4. ESTIMATING CO AND H I VELOCITIES FROM CGPS DATA

A telescope pointed directly towards an H II region is likely to view line-of-sight (LOS) molecular outflows, or a molecular shell's front or back "caps" that are expanding along the LOS. Typical ^{12}CO velocities as published (e.g. Blitz et al. 1982) are almost certainly affected, and thus there may be a significant difference between the object's published velocity and the *systemic*, which we define as free of motions from LOS expansions and outflows, and other systematic effects (e.g. "rolling" motions in the arms). The $1/\sin \ell$ projection from v_{LSR} to angular velocity Ω will amplify any such differences. For Galactic structure and dynamics studies, the ideal is to isolate only the LOS component of an object's orbital motion. CGPS data are advantageous in this regard: the large-scale high-resolution maps allow one to look for the velocity channels where the associated gas is seen *to one side of or around the edges of* the ionized gas, and discriminate against gas seen atop the face of the H II (see Figure 2 for an example). Velocities derived in this way are more likely to reflect only the object's motion about the Galactic centre, and less likely to exhibit peculiar motions along the LOS, whether systematic or random (e.g. "turbulence", cloud-cloud dispersion motions).

Two systemic velocities are estimated independently from CGPS H I and from Exeter FCRAO $^{12}\text{CO}(J=1\rightarrow 0)$ GPS data (Mottram & Brunt 2010; Brunt et al. 2013) for each H II region. High-resolution ^{12}CO data towards Sh2-121, CTB 104b, 124, 127, 128, 129, 131, and 184 are not available and CO velocities are estimated with 8-arcminute ^{12}CO data from Dame et al. (2001). Additional H II regions Sh2-261, and 267–272 are not observed in either ^{12}CO or H I, so only CO velocities from Fich et al. (1989) (where observed) are reported. For each H II region we first overlay 21 cm continuum contours and mark the position of each star on both ^{12}CO and H I channel maps, and search each channel for structure in the gas that correlates with the spatial appearance of the ionized gas and star locations. Channel maps where atomic and molecular gas shells that surround the ionized gas (defined with 21 cm continuum images) are seen *edge-on* (and not *face-on*) are sought. ^{12}CO emission is naturally concentrated into discrete clouds, and it is usually straightforward to identify associated CO around the periphery of an H II region. The ubiquity of H I appearing at all angular scales ($\sim 1'$ and up) and across many velocity channels creates a somewhat more confused picture, where shells, walls and other features may be superposed with ISM clouds, threads and sheets that are rather related to larger scale Galactic structure (e.g. the disk, spiral arms). To enhance our ability to identify in particular H I related to each H II region, we also overlay H α emission contours from the Wisconsin H-Alpha Mapper (WHAM) plus Virginia Tech Spectral-line Survey (VTSS) map (Finkbeiner 2003) for comparison (only where the angular resolution of the WHAM+VTSS map is the nominal $\sim 6'$). A few H II regions show little distinct 21 cm continuum emission above the background (e.g. Sh2-177, BFS 28), so for these we rely solely on H α to delineate the ionized gas boundaries.

In the 1-arcminute data, ^{12}CO is often seen to form crescent-like shells curving partially (e.g. Sh2-173; see Figure 2) or fully (e.g. Sh2-231) around the limb of the ionized gas. The systemic velocity is found from the centre of several channels where the appearance of the

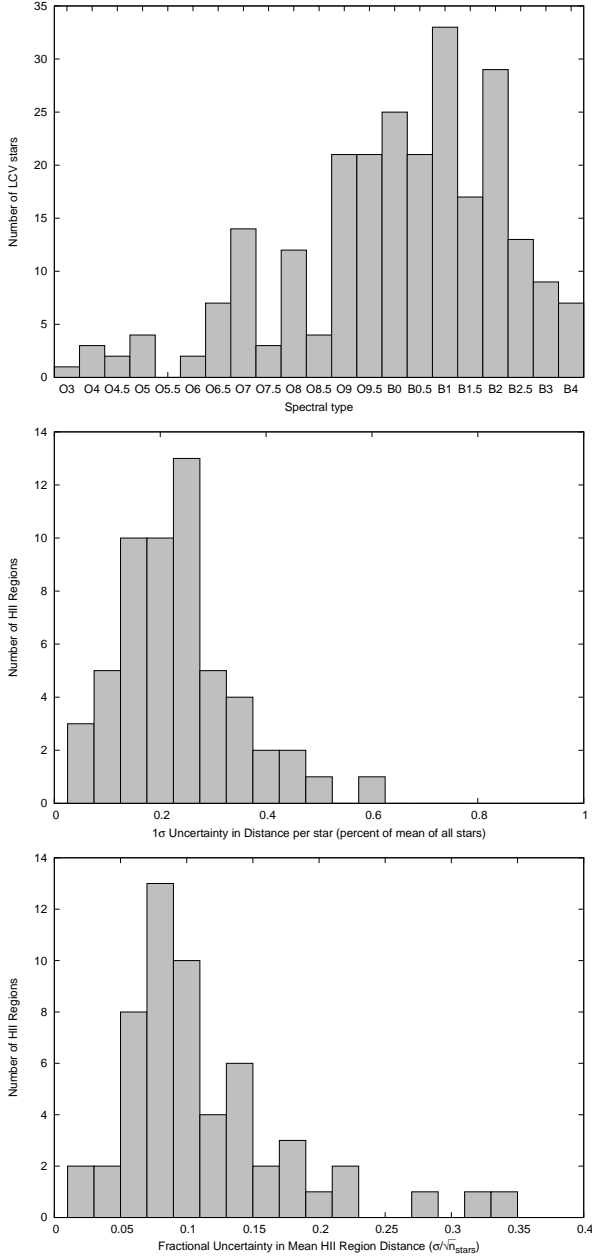


Figure 1. (Top) Number distribution of 248 main-sequence type (LCV) stars in our main catalogue of 103 H II regions, with spectral types O3-B4. (Middle) Distribution of 56 fractional uncertainties in the distance per star in a cluster belonging to an H II region, calculated from the standard deviation of two or more individual stellar distances for the region (σ_*/r). (Bottom) Distribution of 56 fractional uncertainties in the mean distances to the H II region’s cluster, $\sigma_*/\sqrt{n_*}/r$.

edge-on shell is widest and its shape is unchanging from one channel to the next. Often, an imprint of the CO features is seen in the H I channel maps in the form of H I Self-Absorption (HISA; e.g. Sh2-207, Sh2-232) at the same velocities, and in general, at the position around the edge where ^{12}CO is seen, corresponding H I emission from the shell is not. In CGPS H I datacubes we find a wider variety of structures that can be used to narrow down the systemic velocity range. These are broadly categorized below (in order of significance to estimating

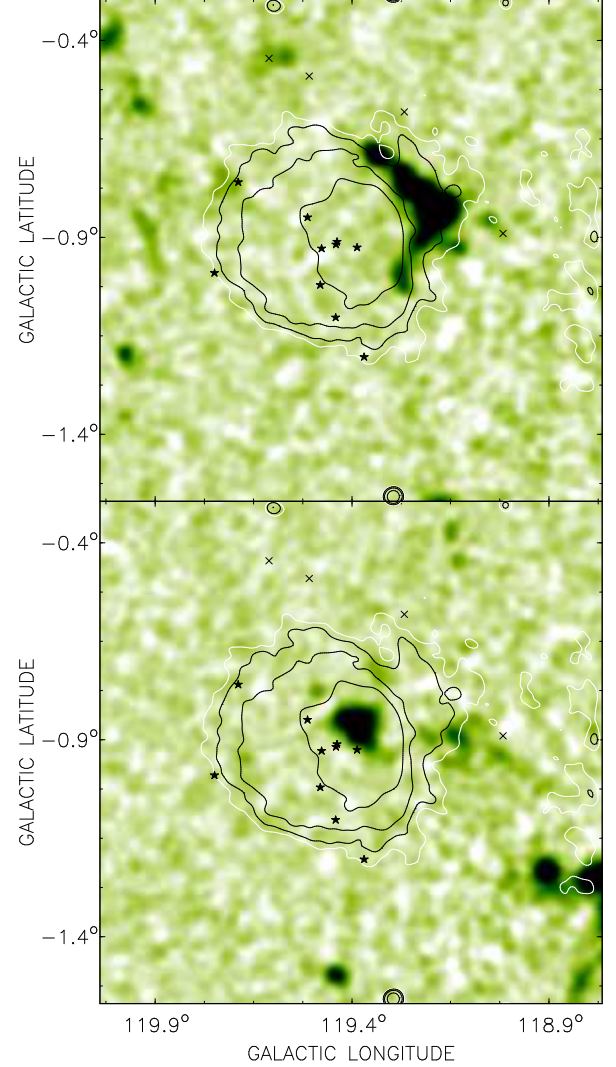


Figure 2. Two velocity channels of ^{12}CO associated with Sh2-173, with 21 cm continuum contours (5.4, 5.45, 5.6, 6 K) overlaid, and the positions of 14 stars associated with the nebula (marked with star symbols), four of which are excluded under criteria i) discussed in Sec. 3 (x-symbols). (Top) A partial ^{12}CO shell seen on the edge of the H II at $v_{\text{LSR}} = -30.7 \text{ km s}^{-1}$. (Bottom) ^{12}CO cloud seen on the face at $v_{\text{LSR}} = -38.2 \text{ km s}^{-1}$. This cloud is more likely to be moving towards or away from the Sun as part of an expanding shell, making its velocity as an indicator of Galactic rotation less reliable than the shell seen edge-on.

a systemic velocity):

1. Thin semi-circular crescents of H I emission contoured around the edges of the ionized gas in a continuous or fragmented arc, and either completely surrounding the H II (e.g. Sh2-207, Sh2-217) or only partially so (e.g. Sh2-168-169, Sh2-204; see Figure 3). Annulus or crescent-like shells appear completely in a small number of velocity channels. The systemic velocity is the mean channel where the shell appears widest and unchanging from one channel to the next.
2. H I appears to consist of an arc-like portion of a shell contoured partway around the H II boundary.

The position of the H I arc around the edge of the H II moves clockwise or anticlockwise around the periphery of the H II from channel to channel. As a result, the velocity-integrated H I emission forms a partial or complete shell around the H II (e.g. Sh2-139, 198, 254).

3. Thick flat “walls” of atomic hydrogen emission with a slight concavity, inside which the H II region appears with one or more stars whose wind(s) probably are shaping one side of the H I wall (e.g. Sh2-124, 143, 164, 202, 227, 231, 249), and producing an H II “blister” off of the H I wall.
4. A clear cavity or depression in H I brightness containing the star(s) (e.g. Sh2-141, Sh2-168) and the H II region(s), perhaps bounded on one side by a thick H I wall or cloud (e.g. Sh2-161, 177, 198,

LBN 676, Sh2-232) or by a thin nearly complete shell of H I emission (e.g. the group Sh2-147 & 148/149).

5. Small HISA features off the limb of the H II (e.g. Sh2-192 & 193, 205, 206, 228, 234, 252), indicating the presence of a cool compressed edge of H I, or on the face of the H II (e.g. Sh2-242), indicating a shell end-cap.
6. H I Continuum Absorption (HICA) of compact unresolved H II regions (e.g. Sh2-121, 138, 156, 211, 255, 258), possibly by shells of dense neutral hydrogen expanding outwards from them (e.g. Kothés & Kerton 2001).

Several examples of the above H I structures are shown in Figure 3. Instead of presenting the more than 200 such figures for each H II region, for reproducibility we offer detailed text descriptions of the observed spatial and velocity structures channel-by-channel for each systemic velocity reported in Table 1. These observing notes are viewable in the Excel version of Table 1 as descriptive comments attached to each velocity measurement in ^{12}CO and H I, in columns 4 & 5 respectively. This table also includes information to reproduce every observation: continuum contour levels to overlay, Galactic coordinates of all 355 stars, as well as the compiled list of stellar distance calculations. Readers interested in reproducing results with our methodology are encouraged to download CGPS 21 cm continuum, ^{12}CO and H I line data cubes (see Sec. 2) and inspect them along with our descriptions in the online Table1.xls to identify an object’s molecular and atomic gas morphologies. The final systemic velocities in each gaseous tracer for each H II region in this paper are given in Table 2 below.

4.1. Estimating the Velocity Uncertainty

Most H II regions in this catalogue have been scrutinized for related H I and ^{12}CO at least three times over the 3 year period of this study, and where more than one potentially associated feature was identified in the datacube we list multiple candidate velocities for each tracer. The velocity differences among multiple identified features are typically 2-5 km s^{-1} except for a few cases (for example Sh2-151, 166, 168-169, 180, G122.6+1.6, G127.1+0.9) where two or more associated H I and/or CO components are found in quite different velocity ranges ($>8 \text{ km s}^{-1}$ different). The above differences reflect the uncertainty inherent in estimating velocities by eye: relating structure in channel maps to

the continuum and $\text{H}\alpha$ morphology is a somewhat subjective process. The average of these independent estimates then is the final systemic velocity measurement reported in Table 2, one for each molecular and atomic gas component ($v_{12\text{CO}}$ and v_{HI} respectively).

The distribution of CGPS velocities $v_{12\text{CO}} - v_{\text{HI}}$ (Figure 4) shows a mean difference of -0.2 km s^{-1} and a 1σ dispersion of 3.0 km s^{-1} , demonstrating good correlation between the different gaseous tracers. Comparison of ^{12}CO velocities with those of 81 matched H II regions in Blitz et al. (1982) shows a mean difference of 0.6 km s^{-1} and $1\sigma = 1.4 \text{ km s}^{-1}$, and between H I (with its broader thermal linewidth) and the ^{12}CO of Blitz et al. (1982) shows a mean of 1.1 km s^{-1} and 1σ width of $\pm 3.6 \text{ km s}^{-1}$. This indicates that small-magnitude extra motions of order $\sim 2\text{-}3 \text{ km s}^{-1}$ exist in the ^{12}CO velocities of Blitz et al. (1982) that are absent from the ones here, probably the kind demonstrated in Figure 2 (outflows and expansions). Because of the presence of these random LOS motions, the mean of ^{12}CO and H I velocities should have somewhat less uncertainty. Indeed, the distribution of differences between CGPS mean CO+H I velocities and the CO velocities in Blitz et al. (bottom panel, Fig. 4) shows a mean of 0.5 km s^{-1} and 1σ variation of $\pm 1.9 \text{ km s}^{-1}$.

This dispersion in the differences of CO and H I velocities ($\pm 3.0 \text{ km s}^{-1}$) is taken as the uncertainty in the systemic velocity for each object in each tracer. This should include variations from random thermal and cloud-cloud motions in each tracer, instrumental linewidths, and typical variations due to the estimation by eye itself, probably the dominant source here. We also recognize that some individual H II regions have less reliable systemic velocities due to multiple velocity components identified in each tracer, so $\pm 3.0 \text{ km s}^{-1}$ is the *minimum* uncertainty in each velocity estimate.

Table 2

Sh2-no. /Name	ℓ ($^{\circ}$)	b ($^{\circ}$)	$v_{12\text{CO}}$ ($\pm 3.0 \text{ km s}^{-1}$)	v_{HI} ($\pm 3.0 \text{ km s}^{-1}$)	r (kpc)	$dr = \sigma_*/\sqrt{n_*}$ (kpc)	n_* stars (# excl.)	$E(B-V)$ (mag) mean of n_*
121	90.23	+1.72	-62.4	-56.7	6.82	0.32	3	2.022

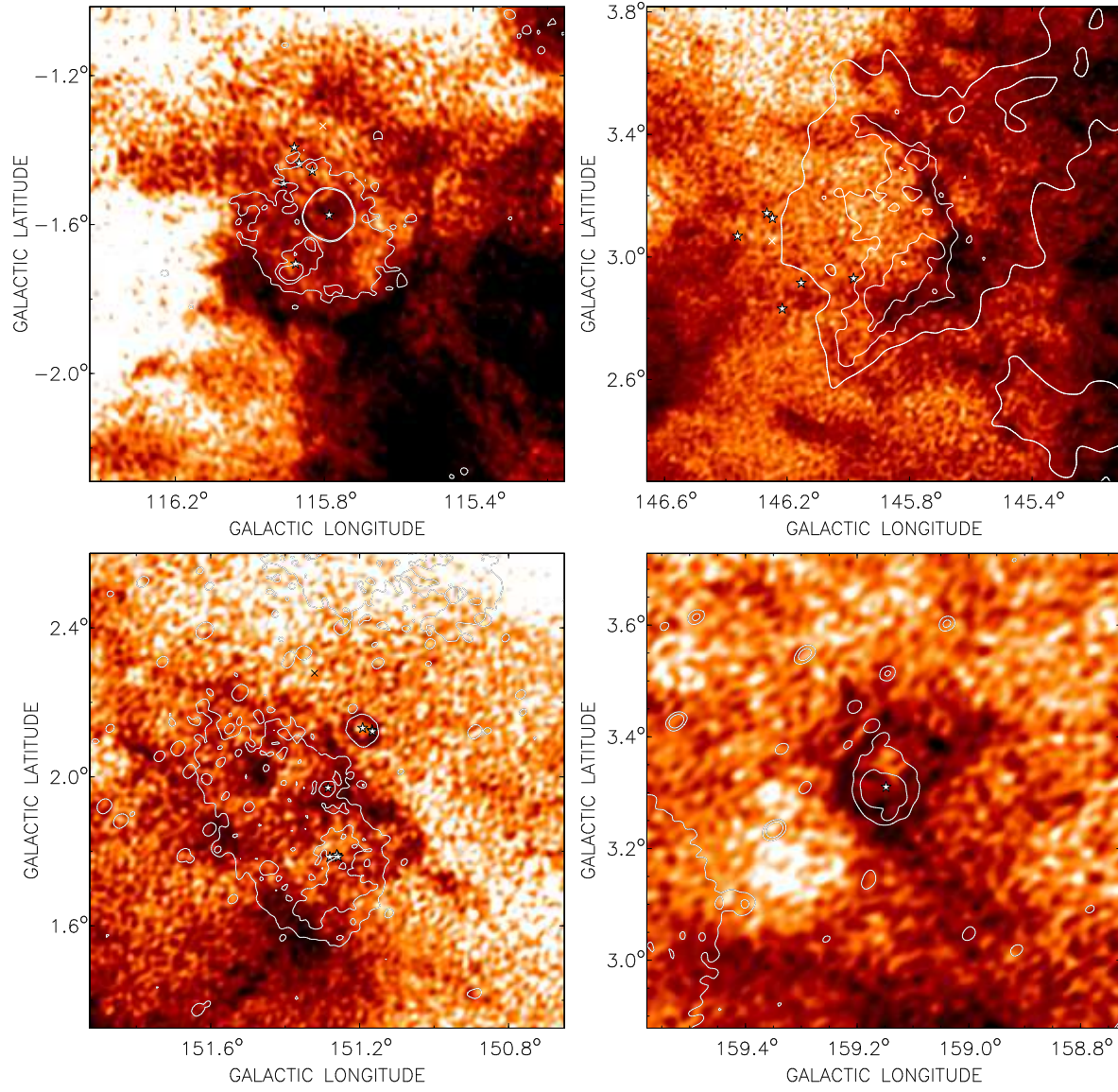


Figure 3. Examples of the partial or complete shells of neutral hydrogen emission seen for many of the H II regions in Table 2. Dark shading corresponds to bright emission, and the positions of associated stars are marked with star symbols. (Top left) A partial semicircular H I shell around the Southern edge of the diffuse emission that surrounds Sh2-168 & Sh2-169 (21 cm contours 5.55, 5.8, 5.9 K) at $v_{LSR} = -34.4 \text{ km s}^{-1}$; (Top right) Partial H I shell surrounding the western edge of Sh2-204 (21 cm contours 4.9, 5.0, 5.1 K), $v_{LSR} = -32.4 \text{ km s}^{-1}$. (Bottom left) Complete and partial shells surrounding Sh2-207 (top right), and Sh2-208 (centre) which is embedded in Waterloo 1 (diffuse extended emission) and the H I surroundings at the same velocity $v_{LSR} = -25.4 \text{ km s}^{-1}$. (Bottom right) Complete H I shell surrounding Sh2-217 (21 cm contours 5.3 & 7 K); $v_{LSR} = -20.4 \text{ km s}^{-1}$.

Table 2 — *Continued*

Sh2-no. /Name	ℓ ($^{\circ}$)	b ($^{\circ}$)	$v_{12\text{CO}}$ ($\pm 3.0 \text{ km s}^{-1}$)	v_{HI} ($\pm 3.0 \text{ km s}^{-1}$)	r (kpc)	$dr = \sigma_*/\sqrt{n_*}$ (kpc)	n_* stars (# excl.)	$E(B - V)$ (mag) mean of n_*
124	94.57	-1.45	-43.55	-41.87	3.78	0.64	2	1.319
CTB104b	94.72	-1.54	-14.95	-14.65	2.36	0.14	5	0.638
127	96.27	+2.57	-94.7	-92.98	9.97	1.99	1	1.73
BFS8	96.35	-0.2	-54.44	-55.47	8.75	1.75	1	1.338
128	97.56	+3.16	-74	-70.72	8.06	1.61	1	1.768
129	99.06	+7.4	+1.42	-6.3	0.81	0.15	5	0.572
G99.1+7.4	99.1	+7.51	-12.6	-8.9	1.29	0.26	1	0.598
131	99.43	+3.66	-1.88	+1.94	1.00	0.08	12	0.500
BFS10	101.44	+2.66	-61.3	-60.82	6.18	1.24	1	1.73
DA568	101.1	+2.5	-64.5	-63.3	4.87	0.04	2	1.084
132	102.96	-0.8	-49.28	-49.28	3.44	0.29	6	0.825
134	103.72	+2.18	-16.3	-17.54	1.63	0.33	1(1)	1.038
135	104.59	+1.37	-20.84	-17.13	1.4	0.28	1	0.955
137	105.63	+8	-8.08	-11.15	0.81	0.17	7	0.27
138	105.62	+0.34	-49.9	-56.7	3.04	0.61	1	2.415

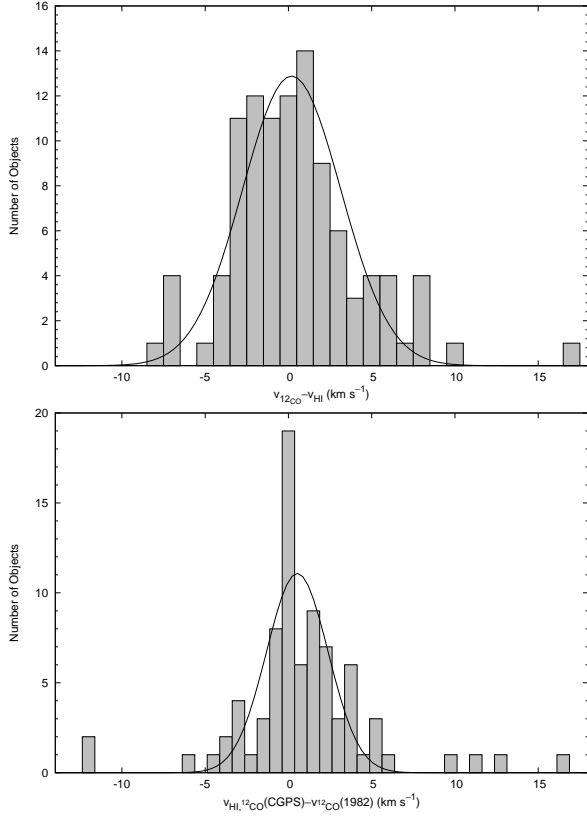


Figure 4. (Top) The distribution of differences between ^{12}CO velocities and H I velocities for all 103 H II regions of our sample. The mean is -0.2 km s^{-1} and the (1σ) dispersion is 3.0 km s^{-1} . (Bottom) Distribution of differences between the mean of our H I and ^{12}CO velocities and ^{12}CO velocities from Blitz et al. (1982) for 81 matching H II regions. The mean difference is 0.5 km s^{-1} and the dispersion is 1.9 km s^{-1} .

Table 2 — *Continued*

Sh2-no. /Name	ℓ ($^\circ$)	b ($^\circ$)	$v_{12\text{CO}}$ ($\pm 3.0 \text{ km s}^{-1}$)	v_{HI} ($\pm 3.0 \text{ km s}^{-1}$)	r (kpc)	$dr = \sigma_*/\sqrt{n_*}$ (kpc)	n_* stars (# excl.)	$E(B - V)$ (mag) mean of n_*
139	105.77	-0.1	-48.87	-52.99	3.22	0.29	3(1)	0.61
140	106.79	+5.31	-8.08	-7.24	0.92	0.16	4	0.823
141	106.81	+3.31	-65.77	-62.89	9.92	1.98	1	1.259
142	107.28	-0.9	-39.19	-39.39	3.48	0.24	9	0.628
143	107.21	-1.34	-33.21	-34.03	3.84	0.77	1	0.655
145	108.18	+5.15	-7.01	-7.44	0.93	0.12	2	1.241
147	108.26	-1.07	-55.05	-51.35	3.13	0.63	1	1.128
148	108.36	-1.06	-55.47	-51.76	3.14	0.63	1	1.24
149	108.39	-1.05	-55.47	-51.76	5.46	1.09	1(4)	0.83
150	108.86	+6.15	-7.94	-10.53	1.02	0.12	2	0.6
151	108.6	-2.74	-53.82	-50.11	3.26	0.26	9	0.71
152	108.76	-0.95	-51.76	-49.28	2.9	0.58	1	1.291
153	108.77	-0.99	-51.76	-50.11	4.6	0.41	2	0.748
154	108.98	+1.59	-8.88	-17.95	1.48	0.3	2	1.349
155	110.22	+2.55	-8.88	-9.71	0.84	0.04	10	0.825
156	110.11	+0.05	-50.9	-48.46	2.68	0.54	1	1.278
BFS17	110.20	+0.01	-50.11	-47.22	2.73	0.55	1	0.855
157	111.2	-0.75	-47.3	-47.43	2.93	0.28	9	0.8
158	111.54	+0.78	-50.93	-50.93	2.44	0.77	2	1.614
159	111.61	+0.37	-54.23	-60	3.07	0.61	1	1.232
160	111.8	+3.73	-10.53	-15.07	0.95	0.09	3	0.749
161	112.1	+1.02	-47.63	-45.57	2.96	0.59	1	1.2
162	112.23	+0.24	-45.16	-52.17	2.41	0.16	2(2)	0.51
163	113.52	-0.57	-43.93	-41.86	3.01	0.41	5(1)	1.132
164	113.91	-1.6	-37.95	-43.51	3.08	0.62	1	1.02
165	114.65	+0.14	-34.44	-35.27	1.96	0.39	1	0.76
166	114.5	-0.86	-48.05	-50.52	2.36	0.47	1(2)	0.988
168	115.79	-1.65	-41.04	-38.57	2.14	0.30	5(1)	0.865
169	115.88	-1.71	-37.74	-38.98	2.09	0.42	1	0.84
170	117.57	+2.26	-46.81	-48.05	2.79	0.33	6(1)	0.649

Table 2 — *Continued*

Sh2-no. /Name	ℓ ($^{\circ}$)	b ($^{\circ}$)	$v_{12\text{CO}}$ ($\pm 3.0 \text{ km s}^{-1}$)	v_{HI} ($\pm 3.0 \text{ km s}^{-1}$)	r (kpc)	$dr = \sigma_*/\sqrt{n_*}$ (kpc)	n_* stars (# excl.)	$E(B - V)$ (mag) mean of n_*
171	118.2	+4.99	-14.65	-15.89	0.91	0.09	7	1.388
173	119.4	-0.84	-32.38	-29.49	2.96	0.31	10(4)	0.53
175	120.36	+1.97	-49.28	-51.76	2.67	0.53	1(2)	1.052
177	120.75	-0.28	-47.22	-45.98	2.37	0.22	6(1)	0.508
180	122.63	+0.09	-43.51	-40.63	5.41	1.08	1	0.77
G122.6+1.6	122.67	+1.45	-55.88	-48.05	2.41	0.15	5	0.7
184	123.15	-6.29	-30.4	-27.02	3.10	0.13	8(1)	0.368
185	123.96	-1.8	-31.69	-31.97	3.23	0.65	1	0.48
186	124.9	+0.1	-41.86	-42.69	2.76	0.15	2	1.07
187	126.67	-0.805	-15.48	-15.48	1.58	0.32	1(1)	1.431
G127.1+0.9	127	+0.84	-47.43	-46.8	2.15	0.43	1	0.62
190	133.71	+1.21	-42.69	-42.28	2.00	0.13	8(1)	0.825
192	136.13	+2.08	-46.81	-50.11	3.49	0.7	1	0.946
193	136.14	+2.12	-45.98	-51.76	2.44	0.49	1(1)	0.76
196	136.44	+2.54	-45.16	-47.63	5.52	1.1	1	0.835
G137.8-1.0	137.77	-0.95	-103.7	-102.46	6.93	1.39	1	1.021
198	137.38	+0.2	-44.75	-40.01	2.49	0.5	1(2)	0.95
199	137.7	+1.6	-37.75	-34.03	1.76	0.14	8(1)	0.645
LBN676	139.66	+2.54	-42.69	-43.51	3.5	0.7	1	0.95
202	139.99	+2.09	-10.33	-14.66	0.97	0.08	5(1)	0.586
G140.8+3.1	140.8	+3.06	-8.88	-10.53	0.6	0.12	1	0.708
BFS28	141.73	+2.76	-11.05	-11.77	0.73	0.12	2(1)	0.499
203	143.75	-1.75	-32.38	-33.21	1.79	0.36	1	1.391
BFS31	143.82	-1.57	-31.88	-30.73	1.75	0.35	1	0.73
204	145.83	+2.94	-36.95	-32.79	3.76	0.14	6(2)	0.653
205	148	-0.4	-6.48	-14.24	0.85	0.15	3(2)	0.607
206	150.61	-0.93	-23.75	-21.67	3.02	0.6	1	1.356
207	151.21	+2.11	-25.78	-28.88	4.27	1.19	2(1)	1.06
208/Wat 1	151.29	+1.97	-30.1	-25.79	4.44	0.55	4(3)	0.89
209	151.61	-0.24	-48.87	-50.11	10.58	0.57	3	1.676
211	154.65	+2.46	-37.97	-37.33	7.39	0.44	3	1.664
212	155.36	+2.615	-34.41	-37.12	4.81	0.6	4(1)	0.867
217	159.15	+3.27	-20.43	-20.84	4.37	0.87	1	0.725
219	159.36	+2.57	-25.37	-23.72	4.23	0.64	2(1)	0.849
223	166.2	+2.54	-22.49	-20.02	4.05	0.81	1	0.66
225	168.09	+3.07	-22.49	-23.73	3.79	0.76	1	0.721
227	168.68	+1.09	-19.33	-17.54	4.08	0.82	1(3)	0.831
228	169.19	-0.9	-13.01	-14.65	4.2	0.3	2	1.4
229	172	-2.2	-3.11	+4.72	0.73	0.24	2	0.491
231	173.47	+2.55	-18.92	-18.16	2.12	0.42	1	1.131
232	173.5	+3.1	-12.83	-11.63	2.09	0.42	1(1)	0.565
234	173.38	-0.19	-8.51	-12.8	2.19	0.1	13	0.54
235	173.62	+2.81	-17.4	-16.72	1.36	0.27	1	1.18
236	173.6	-1.78	-3.81	-20.22	4.03	0.32	7(1)	0.54
237	173.97	+0.25	-4.7	-12.46	3.76	0.28	3	0.723
241	180.79	+4.03	-6.41	-12.19	4.84	0.97	1	0.621
242	182.36	+0.19	+1.42	+2.65	2.19	0.44	1	0.74
247	188.96	+0.85	+2.65	+1.83	2.23	0.18	2	0.978
249	189.45	+4.38	+0.18	+8.84	2.01	0.15	5	0.555
252	189.81	+0.33	+8.02	+12.55	2.23	0.14	11	0.633
253	192.23	+3.59	+14.63	+12.55	4.29	0.37	8(1)	0.525
254	192.44	-0.21	+12.55	+14.61	2.43	0.49	1	0.645
255	192.63	-0.02	+12.55	+11.72	2.27	0.45	1	1.18
256	192.60	-0.13	+7.6	+14.61	2.59	0.52	1	1.345
257	192.58	-0.08	+7.6	+11.31	2.16	0.43	1	0.865
258	192.72	+0.04	+8.02	+15.85	3.03	0.61	1	1.398
259	192.91	-0.62	+22.86	+23.68	8.71	1.74	1	1.228
Additional H II regions beyond CGPS								
261	194.148	-2.037	-	-	1.89	0.38	1	0.61
267	196.188	-1.177	-	-	3.89	0.28	2	1.123
268	196.38	-2.85	4.8	-	3.26	0.07	3	0.697
269	196.45	-1.68	17.5	-	4.27	0.85	1	1.365
270	196.83	-3.10	25.6	-	9.27	1.85	1	1.07
271	197.8	-2.33	20.5	-	3.90	0.47	1	0.98
272	196.83	-2.33	20.6	-	4.96	0.99	1	0.938

5. COMPARISON WITH PREVIOUS STUDIES

Like the more recent catalog of Russeil (2003), we present a homogeneous set of new stellar distances to 103 H II regions derived using a common LC and colour calibration for stars. Our approach is more fundamen-

tal, however, in that we use high-resolution radio maps to define the outermost boundary of the H II emission and then consider (or reconsider) all known OB stars in the area, excluding those outside of the emission bounds or outside a distance range that is common to the others. This data mining has greatly increased the number

of individual SFRs with consistently calculated stellar distance estimates in quadrants II and part of III: for example, the compilation of Hou et al. (2009) lists only 56 single or group distances for 71 objects in the longitude range of the CGPS.

Nine high-mass SFRs with distances and uncertainties measured via VLBI observations of trigonometric parallax can be matched to H II regions in the CGPS (Figure 5; top). The error-weighted correlation between these distances ($r_\pi \pm dr_\pi$) and our stellar distances (plotted in Figure 5) is $r_\pi = 0.999 \pm 0.054 r - 0.126 \pm 0.070$, essentially 1:1 within a distance range up to $r \lesssim 4.5$ kpc. Although not within the CGPS region, we also include our stellar distance to Sh2-269 of $r = 4.3 \pm 20\%$ kpc (from the lone B0.5V star found by Moffat et al. 1979, see “Additional H II regions beyond CGPS” in Table 2 and online Table 1) and use the recent parallax results of Asaki et al. (2014): $r_\pi = 4.05^{+0.65}_{-0.49}$ kpc.

5.1. Improvements

Improvements in the distances and velocities of H II regions will translate into a clearer view of Galactic structure and dynamics. These improvements can be assessed by measuring the scatter in Galactocentric distance R and angular velocity relative to the Sun $\Omega - \Omega_0$ (Eqn. 1 in Foster & Cooper 2010) in spiral arm objects, both values for which are expected to be (nearly) constant across a (nearly) circular ring about the Galactic centre (assuming the pitch angle of the arm is small and only a short segment of the arm is considered). We have 34 Perseus spiral arm H II regions between $90^\circ \lesssim \ell \lesssim 150^\circ$ (see Paper II Foster & Brunt 2013, for this determination). We compare distances R_{Per} from our catalogue to the compilation of Hou et al. (2009), which has 19 objects in common (velocities and distances mainly referenced from Paladini et al. 2003; Fich et al. 1989; Russeil 2003; Russeil et al. 2007). Eight additional objects with stellar distances and CO velocities are found in Blitz et al. (1982). A value for the Solar galactocentric distance $R_0 = 8$ kpc (Foster & Cooper 2010) is assumed. Some objects in Hou et al. (2009) are “grouped” together into 2 entries with duplicated distances and velocities. For proper comparison to our data (which is not grouped) we remove one member of the Sh2-148/149 and Sh2-203/BFS 31 groups from the comparison (149,203), and replace one member in 3 other groups (Sh2-138/139, 152/153 and 158/159) with alternate stellar distances and velocities from Blitz et al. (1982). We also remove the distance outliers BFS 8 and Sh2-180 from both datasets.

Two plots of $\Omega - \Omega_0$ vs. R_{Per} for the 23 remaining objects are shown in Figure 5, one made with previous catalogue data and the other from data in Table 2. Visually, the results of the current study cluster together much tighter in each variable as compared to previous catalogue values. A robust direct comparison of the median and normalized median absolute deviations in R_{Per} using distances in Hou et al. (2009); Blitz et al. (1982) show $R_{Per} \simeq 9.48 \pm 0.42$ kpc, whereas for the same regions in our data $R_{Per} \simeq 9.47 \pm 0.17$ kpc; essentially the same median distance to the Perseus arm but with significantly lower relative scatter. In the comparison of angular velocities, a mean and 1σ scatter of $\Omega - \Omega_0 =$

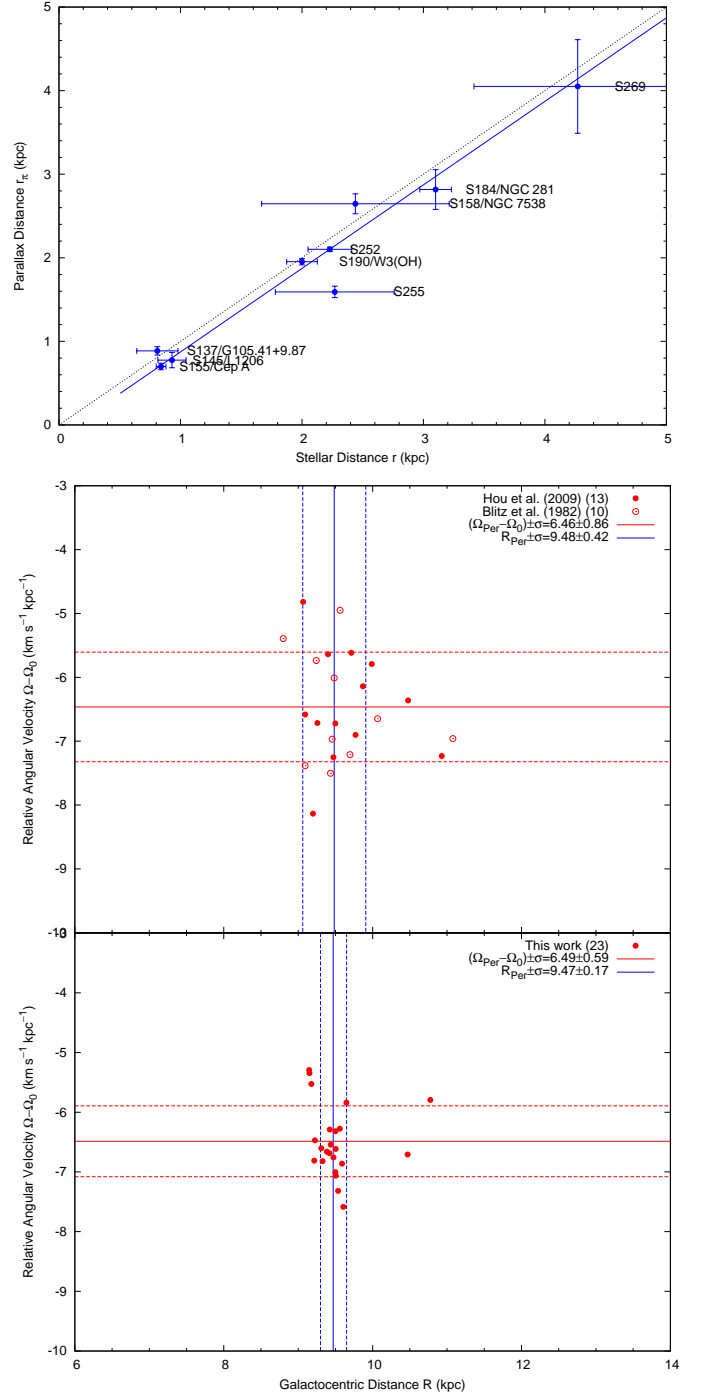


Figure 5. (Top) Comparison of our stellar distances to parallax distances r_π for 9 H II regions in the CGPS matched with masers observed with VLBI. References are Reid et al. (2009) (Cep A, NGC 7538, NGC 281, W3(OH), Sh2-252), Rygl et al. (2010) (L1206 and Sh2-255), Xu et al. (2013) (Sh2-137/G105.41+9.87) and Asaki et al. (2014) (Sh2-269). (Centre and Bottom) Comparison of Galactocentric distances and angular velocities for 23 Perseus spiral arm H II regions, calculated with heliocentric distances and LSR velocities from Hou et al. (2009) and Blitz et al. (1982) (centre) and from Table 2 here (bottom). Dashed lines indicate the 1σ (standard deviation) of the sample in each axis. See Sec. 5.1.

$-6.455 \pm 0.857 \text{ km s}^{-1} \text{ kpc}^{-1}$ for the Perseus spiral arm is found for the 23 objects catalogued by Hou et al. (2009) and Blitz et al. (1982); Fich et al. (1989). Referenced velocities in Hou et al. (2009) are a mix of CO and radio recombination line (Paladini et al. 2003); if we restrict the comparison to strictly ^{12}CO velocities from Blitz et al. (1982); Fich et al. (1989) the scatter is $\pm 0.809 \text{ km s}^{-1} \text{ kpc}^{-1}$. Using CGPS ^{12}CO velocities alone the scatter is reduced to $\pm 0.592 \text{ km s}^{-1} \text{ kpc}^{-1}$, and with CGPS H I it is $\pm 0.686 \text{ km s}^{-1} \text{ kpc}^{-1}$. Taking the mean between the two gaseous tracers (weighted by $1/\sigma^2$) results in $-6.486 \pm 0.593 \text{ km s}^{-1} \text{ kpc}^{-1}$, a factor of $\approx 1/\sqrt{2}$ less scatter in $\Omega - \Omega_0$ than in the same sample from previous catalogues. In particular, using ^{12}CO velocities in this work also produces $\sim 1/\sqrt{2}$ less scatter than using those from Blitz et al. (1982). Clearly, the technique of estimating the systemic velocity from related gas seen edge-on results in a dataset better for studying Galactic dynamics, having reduced the variations due to random (e.g. “turbulence” and cloud-to-cloud motions) as well as expansion and outflow motions along the LOS.

In summary, the new distances and CGPS velocities presented in this paper do indeed have favourable characteristics for use in tracing Galactic structure and dynamics, and have an edge in terms of lower scatter when compared to existing data in the literature.

We would like to thank the referees for their careful reading of and thoughtful comments on our manuscript. The Dominion Radio Astrophysical Observatory is operated as a national facility by the National Research Council of Canada. The Canadian Galactic Plane Survey has been a Canadian project with international partners, and was supported by grants from the Natural Sciences and Engineering Research Council of Canada (NSERC). The Five College Radio Astronomy Observatory was supported by NSF grant AST 0540852. TF has been supported by an NSERC Discovery grant and a Brandon University Research Committee Grant. CB is funded in part by the UK Science and Technology Facilities Council grant ST/J001627/1 (“From Molecular Clouds to Exoplanets”) and the ERC grant ERC-2011-StG_20101014 (“LOCALSTAR”), both held at the University of Exeter.

REFERENCES

- Asaki, Y., Imai, H., Sobolev, A. M., Parfenov, S. Yu. 2014, *ApJ*, 787, 54
- Avedisova, V. S. & Kondratenko, G. I. 1984, *Nauchnye Informatsii*, 56, 59
- Binney, J. & Dehnen W. 1997, *MNRAS*, 287, 5
- Blitz, L., Fich, M., & Stark, A. A. 1982, *ApJS*, 49, 183
- Brand, J., & Blitz, L. 1993, *A&A*, 275, 67
- Brunt, C. M., Heyer, M., Mottram, J. C., Douglas, K. A. & Summers, L. 2013, in prep.
- Brunthaler, A., Reid, M. J., Menten, K. M., Zheng, X.-W., Bartkiewicz, A., Choi, Y. K., Dame, T., Hachisuka, K., Immer, K., Moellenbrock, G., Moscadelli, L., Rygl, K. L. J., Sanna, A., Sato, M., Wu, Y., Xu, Y. and Zhang, B. 2011, *Astron. Nachr.*, 332, 461
- Chan, G., & Fich, M. 1995, *AJ*, 109, 2611
- Chini, R. & Wink, J. E. 1984, *A&A*, 139, L5
- Churchwell, E., Babler, B. L., Meade, Whitney, B. A., Benjamin, R., Indebetouw, R., Cyganowski, C., Robitaille, T. P., Povich, M., Watson, C., & Bracker, S. 2009, *PASP*, 121, 213
- Crampton, D., Georgelin, Y. M., & Georgelin, Y. P. 1978, *A&A*, 66, 1
- Crampton, D., & Fisher, W. A. 1974, *Publications of the Dominion Astrophysical Observatory Victoria*, 14, 283
- Dame, T. M., & Thaddeus, P. 2011, *ApJ*, 734, L24
- Dame, T. M., Hartmann, D., & Thaddeus, P. 2001, *ApJ*, 547, 792
- Deharveng, L., Zavagno, A., Nadeau, D., Caplan, J., & Petit, M. 1999, *A&A*, 344, 943
- Dewdney, P. E., Roger, R. S., Purton, C. R., & McCutcheon, W. H. 1991, *ApJ*, 370, 243
- Drimmel, R., & Spergel, D. M. 2001, *ApJ*, 556, 181
- Erickson, N. R., Grosslein, R. M., Erickson, R. B., & Weinreb, S. 1999, *IEEE Trans. Microwave Theory Tech.*, 47, 2212
- Feitzinger, J. V. & Spicker, J. 1985, *MNRAS*, 214, 539
- Fich, M., Dahl, G. P. & Treffers, R. R. 1990, *AJ*, 99, 622
- Fich, M., Blitz, L., & Stark, A. A. 1989, *ApJ*, 342, 272
- Finkbeiner, D. P. 2003, *ApJS*, 146, 407
- Fitzpatrick, E. L. & Massa, D. 2007, *ApJ*, 663, 320
- Foster, T. & Brunt, C. 2013, in prep. (Paper II)
- Foster, T. & Cooper, B. 2010, in *ASP Conf. Ser.* 438, *The Dynamic Interstellar Medium: A Celebration of the Canadian Galactic Plane Survey*, ed. R. Kothés, T. L. Landecker & A. G. Willis (San Francisco, CA:ASP), 16
- Georgelin, Y. M. & Georgelin, Y. P. 1976, *A&A*, 49, 57
- Georgelin, Y. M., Georgelin, Y. P. & Roux, S. 1973, *A&A*, 25, 337
- Georgelin, Y. P. & Georgelin, Y. M. 1970, *A&A*, 6, 3490
- Glushkov, Yu. I. 1995, *Astronomical and Astrophysical Transactions*, 8, 105
- Guetter, H. H., & Turner, D. G. 1997, *AJ*, 113, 2116
- Henden, A. A., & Kaitchuck, R. H. 1990, *Astronomical Photometry*, Richmond, VA, Willmann-Bell, Inc.
- Heyer, M. H., Brunt, C. M., Snell, R. L., Howe, J., Schloerb, F. P., & Carpenter, J. C., 1998, *ApJS*, 115, 241
- Hill, P. W. & Lynas-Gray, A. E. 1977, *MNRAS*, 180, 691
- Hou, L. G., Han, J. L. & Shi, W. B. 2009, *A&A*, 499, 473
- Hunter, D. A. & Massey, P. 1990, *AJ*, 99, 846
- Jackson, J. M., Rathborne, J. M., Shah, R. Y., Simon, R., Bania, T. M., Clemens, D. P., Chambers, E. T., Johnson, A. M., Dormody, M., Lavoie, R., & Heyer, M. H., 2006, *ApJS*, 163, 145
- Kimeswenger, S. & Weinberger, R. 1989, *A&A*, 209, 51
- Kothés, R., & Kerton, C. R. 2002, *A&A*, 390, 337
- Kutner, M. L., & Ulich, B. L., 1981, *ApJ*, 250, 341
- Lahulla, J. F. 1987, *AJ*, 94, 1062
- Lahulla, J. F. 1985, *A&AS*, 61, 537
- Martin, N. 1972, *A&A*, 17, 253
- Massey, P., Johnson, K. E., & Degioia-Eastwood, K. 1995, *ApJ*, 454, 151
- Mayer, P. & Macák, P. 1973, *BAICz*, 24, 50
- McClure-Griffiths, N. M., Dickey, J. M., Gaensler, B. M., & Green, A. J. 2004, *ApJ*, 607, L127
- Miyoshi, M., Asaki, Y., Wada, K., & Imai, H. 2012, *New Astronomy*, 17, 553
- Moffat, A. F. J., Fitzgerald, M. P., & Jackson, P. D. 1979, *A&AS*, 38, 197
- Mottram, J. C. & Brunt, C. M. 2010, in *ASP Conf. Ser.* 438, *The Dynamic Interstellar Medium: A Celebration of the Canadian Galactic Plane Survey*, ed. R. Kothés, T. L. Landecker & A. G. Willis (San Francisco, CA:ASP), 98
- Negueruela, I. & Marco, A. 2003, *A&A*, 406, 119
- Paladini, R., Davies, R. D., & DeZotti, G. 2004, *MNRAS*, 347, 237
- Paladini, R., Burigana, C., Davies, R. D., Maino, D., Bersanelli, M., Cappellini, B., Platania, P., & Smoot, G. 2003 *A&A*, 397, 213
- Pecaut, M. J., Mamajek, E. E. & Bubar, E. J. 2012, *ApJ*, 746, 154
- Reid, B. C. 2003, *AJ*, 125, 2531
- Reid, M. J., Menten, K. M., Zheng, X. W., Brunthaler, A., Moscadelli, L., Xu, Y., Zhang, B., Sato, M., Honma, M., Hirota, T., Hachisuka, K., Choi, Y. K., Moellenbrock, G. A. & Bartkiewicz, A. 2009, *ApJ*, 700, 137
- Roberts, W. W. 1972, *ApJ*, 173, 259
- Russeil, D. Adami, C., & Georgelin, Y. M. 2007, *A&A*, 470, 161
- Russeil, D. 2003, *A&A*, 397, 133
- Rygl, K. L. J., Brunthaler, A., Reid, M. J., Menten, K. M., van Langevelde H. J., & Xu, Y. 2010, *A&A*, 511, A2
- Sharpless, S. 1959, *ApJS*, 4, 257

- Sota, A., Maíz Apellániz, J., Walborn, N. R., Alfaro, E. J., Barbá, R. H., Morrell, N. I., Gamen, R. C., & Arias, J. I. 2011, *ApJS*, 193, 24
- Sternberg, A., Hoffmann, T. L. & Pauldrach, A. W. A. 2003, *ApJ*, 599, 1333
- Strasser, S. T., Dickey, J. M., Taylor, A. R., Boothroyd, A. I., Gaensler, B. M., Green, A. J., Kavars, D. W., Lockman, F. J., Martin, P. G., McClure-Griffiths, N. M., Rothwell, T. A., & Stil, J. M. 2007, *AJ*, 134, 2252
- Taylor, A. R., Gibson, S. J., Peracaula, M., Martin, P. G., Landecker, T. L., Brunt, C. M., Dewdney, P. E., Dougherty, S. M., Gray, A. D., Higgs, L. A., Kerton, C. R., Knee, L. B. G., Kothes, R., Purton, C. R., Uyaniker, B., Wallace, B. J., Willis, A. G., & Durand, D. 2003, *AJ*, 125, 3145
- Taylor, J. H. & Cordes, J. M. 1993, *ApJ*, 411, 674
- Vallée, Jacques P. 2008, *AJ*, 135, 1301
- Vallée, Jacques P. 2005, *AJ*, 130, 569
- Vázquez, R., May, J., Carraro, G., Bronfman, L., Moitinho, A., & Baume, G. 2008, *ApJ*, 672, 930
- Wegner, Walter. 1994, *MNRAS*, 270, 229
- Wramdemark, S. 1981, *A&AS*, 43, 103
- Xu, Y., Li, J. J., Reid, M. J., Menten, K. M., Zheng, X. W., Brunthaler, A., Moscadelli, L., Dame, T. M. & Zhang, B. 2013, *ApJ*, 769, 15
- Xu, Y., Reid, M. J., Zheng, X. W. & Menten, K. M. 2006, *Science*, 311, 54